Chemical control over hemi-indigo photoswitches

Duindam, N.

CHAPTER 5

Hemi-Indigiosin: a pH and Red-Light Responsive Transmembrane HCl Transporter

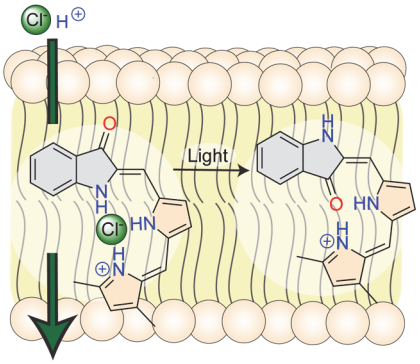

Synthetic anion transporters have emerged as promising therapeutic agents. However, their targeting ability is still low. Herein, we present hemi-indigiosin, which is structurally related to prodigiosin – a well-studied natural product exhibiting a wide range of biological activities. Our hemi-indigiosin is shown to have similar HCl transport selectivity and pH-dependent activity as prodigiosin, while in addition, it can be deactivated by irradiation with visible light. This deactivation is effective due to high photoconversion from the active chloride-binding *Z*-isomer to the inactive *E*-isomer, which lacks a chloride binding site. Transport activity is thus controlled by both pH change and light, which will allow improved targeting of pathological sites, and prevent ecological impact after drug excretion into the environment.

The work that is described in this chapter has been published:

N. Duindam, J. E. Bos, F. van Nifterik, S. J. Wezenberg, *Angew. Chem Int. Ed.* **2025**, e15930.

5.1 Introduction

Artificial molecular systems that facilitate passive anion transport across biological membranes have emerged as promising therapeutic agents.[1-3] These systems may one day be used to take over the function of malfunctioning transport proteins as therapy for channelopathies[4-6] while, furthermore, their ability to trigger cell death through disruption of ion homeostasis could be leveraged for anticancer or antibacterial treatment.[7-10] In the pursuit of novel anticancer agents, the natural product prodigiosin, a remarkably active HCl transporter,[11-13] inspired the design of many new transporters, including tambjamines,[8] obatoclax,[14] and perenosins.[15-16] For the latter compound class, like for prodigiosin,[11] higher transport activity was observed at slightly acidic pH, which could impose selectivity towards cancer cells (tumors have an acidic microenvironment).[1-3,15,16] Also, other transporters responsive to pH, either based on binding site (de)protonation,[17-22] or conformational changes[23-24] have been reported. Nevertheless, poorly targeted cytotoxicity of anticancer drugs causes undesirable side effects and, after excretion of the drug, negative environmental effects persist. That is, anticancer drugs in wastewater pose a potential ecological risk.[25]

The incorporation of molecular photoswitches into drugs has proven promising to control biological activity on demand with high spatiotemporal precision.[26-27] This approach can be used to reduce undesired drug activity away from the pathological site, as well as to diminish environmental toxicity. For example, photoswitchable antibiotics have been developed to combat antimicrobial resistance,[28-29] and photoswitchable anticancer agents have shown potential as precision-targeted chemotherapeutics.[30] In recent years, a similar strategy has been applied to synthetic anionophores to switch between states with high and low transport activity.[31-38] However, to achieve complete deactivation upon light irradiation, quantitative conversion to an inactive isomer is required, which poses a major challenge. Most light-responsive transporters developed so far maintain a significant amount of active form at photoequilibrium. Also, as they commonly rely on a photoswitchable core interconnecting two binding sites (*viz.* molecular tweezers), a binding site is exposed in the low activity form, leading to considerable residual transport. Furthermore, UV light is most frequently used to induce the photoresponse, limiting biological application as it is damaging to cells and has low tissue penetration depth.[26-27]

Hence, we envisioned a transporter in which the binding site is blocked by intramolecular interactions in one state,[39-41] where photoconversion to this state is nearly quantitative.[42] These requirements led us to explore the hemi-indigo scaffold, as it already contains an NH hydrogen bond donor, and its *Z*-isomer can be adapted to resemble prodigiosin when

functionalized with an appropriate dipyrrin moiety (Scheme 1A). Photoisomerization to the *E*-isomer, induced by visible light, would block the dipyrrin binding motif through intramolecular hydrogen bonding with the carbonyl oxygen. Moreover, based on recent work on *N*-heterocyclic hemi(thio)indigo dyes,[43-46] irradiation was expected to lead to high conversion to the intramolecularly hydrogen-bonded species, irrespective of the visible-light wavelength used. As an additional feature of interest, the envisioned light-responsive prodigiosin analog was expected to show pH-dependent activity, since protonation of the dipyrrin fragment is key in prodigiosin-mediated HCl transport across the membrane.[11-13] This type of transporter would thus be responsive to endogenous (pH) as well as exogenous (light) stimuli, and such dual responsivity could further increase the level of control over transport activity.

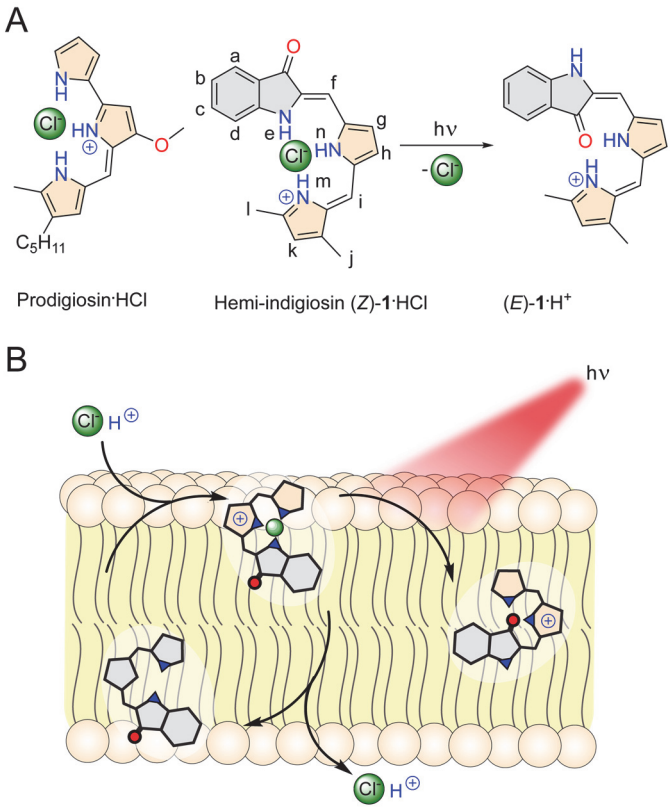

Scheme 1. (A) Structures of the HCl complexes of prodigiosin and the photoresponsive hemi-indigiosin analog (*Z*)-**1**, which undergoes *Z*-to-*E* isomerization in response to visible light. (B) Schematic representation of electroneutral HCl transport across the bilayer membrane by (*Z*)-**1** and deactivation of this transport by photoisomerization to (protonated) (*E*)-**1**.

Herein, we present hemi-indigiosin (*Z*)-**1**, which shows pH and red-light responsivity (see Scheme 1B). It is found to be highly selective for electroneutral HCl over electrogenic Cl^- transport, with higher activity at lower pH value. Near quantitative *Z*-to-*E* isomerization is achieved upon irradiation with visible light, leading to deactivation of HCl transport. To our knowledge, this system represents the first visible-light-switchable transporter with demonstrated HCl selectivity. We envision the combined pH and red-light responsivity to be an important step toward the development of anionophores into therapeutics with high targeting efficiency.

5.2 Energy Minimization by DFT

To validate formation of a suitable chloride-binding pocket in the *Z*-isomer and intramolecular hydrogen bonding in the *E*-isomer, DFT calculations were performed at the B3LYP-D3/aug-cc-pVTZ level of theory using an IEFPCM MeOH solvation model. The energy-minimized structure of (*Z*)-**1**·HCl shows three hydrogen bonds between the N-H protons and the chloride anion [N(H)···Cl distances of 3.142, 3.359, and 3.119 Å, Figure 1A]. The lowest-energy conformer of (*E*)-**1**·H^+ displays two intramolecular hydrogen bonds between the N-H atoms of the protonated dipyrrin unit and the carbonyl oxygen of the indigo fragment [N(H)···O distances of 2.637 and 3.128 Å, Figure 1B]. Also, the structure of (*Z*)-**1**·H^+ was optimized, and its lowest-energy conformer was found to be 20.6 kJ mol^{-1} higher in Gibbs free energy than that of (*E*)-**1**·H^+. These calculations thus confirm that a suitable binding site with three N-H hydrogen bond donors is available in the *Z*-isomer, while interaction of chloride with the two N-H donors of the protonated dipyrrin moiety is restricted in the *E*-isomer.

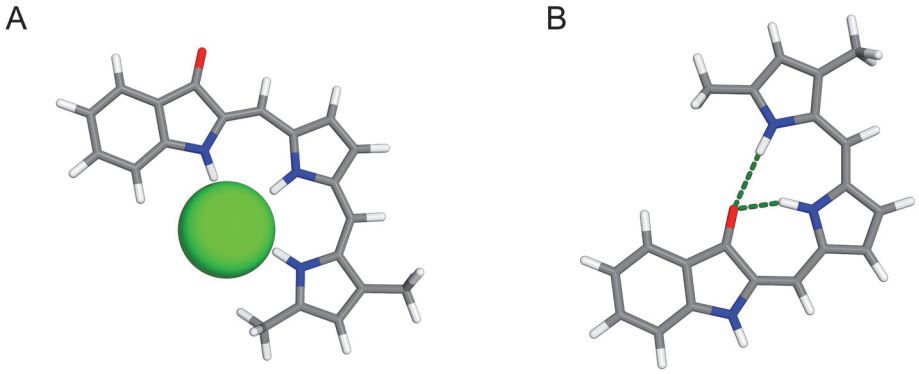

Figure 1. DFT energy-minimized geometries (B3LYP-D3/aug-cc-pVTZ, IEFPCM MeOH) of (*Z*)-**1**·HCl (A) and (*E*)-**1**·H^+ (B) shown in stick representation (with chloride in space-filling representation); Color codes: Hydrogen bond, Cl = green; O = red; N = blue.

5.3 Synthesis

Isomer (*Z*)-**1** was then synthesized starting from the known 2-pyrrole-derived hemi-indigo (**2**, Scheme 2).[47] Synthetic routes towards dipyrrins often employ a MacDonald-type condensation of a pyrrole fragment with 5-formyl pyrrole in the presence of strong acid.[48] In our case, however, such a procedure afforded the product in only trace amounts (Table E1), which is ascribed to the low nucleophilicity of the 2-pyrrole-derived hemi-indigo precursor. Nevertheless, when in a different procedure $POCl_3$ was used to mediate the condensation,[48-51] the conversion improved. The product was isolated by precipitation followed by lyophilization, both in the presence of TFA, to obtain (*Z*)-**1**·TFA in 62% yield as the TFA salt (as confirmed by ^{19}F NMR spectroscopy and elemental analysis, see the Experimental Section).

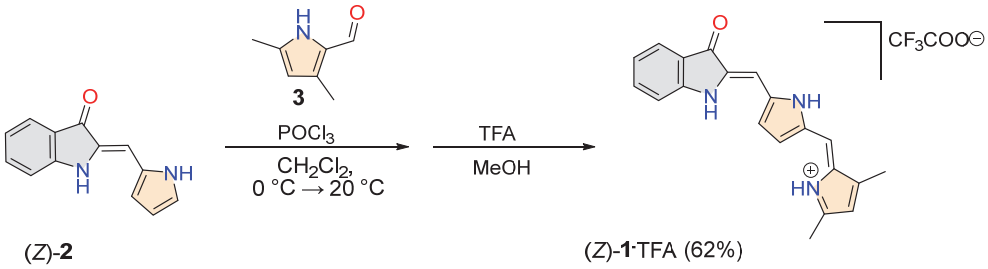

Scheme 2. Synthetic route toward hemi-indigo (*Z*)-**1**·TFA.

5.4 Photoisomerization and Anion Binding Properties

The photoisomerization behavior was first studied by UV-Vis spectroscopy. Therefore, the as-isolated (*Z*)-**1**·TFA salt was dissolved in MeOH, to which some TFA (12 equiv.) was added to ensure quantitative protonation (Figure E1). As can be observed in the spectrum in Figure 2A, the compound absorbs in the visible light region (λ_{max} = 452 and 608 nm). Irradiation of the solution with 599 nm light resulted in a bathochromic shift of the absorbance (λ_{max} = 461 and 655 nm, Figure 2B), characteristic of hemi-indigo *Z*-to-*E* isomerization.[43-46,52] The spectrum recorded at PSS only minimally changed over the course of 1 h in the dark (Figure E1), indicating high thermal stability of the photogenerated *E*-isomer. Interestingly, when subsequently irradiating the sample with 455 nm light, around the maximum where the *E*-isomer has higher absorption than the *Z*-isomer, the spectrum almost did not change, indicating that a similar photostationary state (PSS) ratio was attained. During irradiation, a clear isosbestic point was maintained at λ = 638 nm (Figure 2). Also, when subsequently irradiating close to this isosbestic point with 637 nm light, only minor spectral changes were observed. Hence, these UV-Vis studies indicate that similar PSS ratios are obtained at the

used irradiation wavelengths (i.e., 599, 455, and 637 nm). When using a high-power LED emitting around 730 nm, only minor isomerization back to the *Z*-isomer was noted in the UV-Vis spectrum after 1 h of continuous irradiation, which is much longer than the time that was needed to reach PSS599 (Figure 2B).

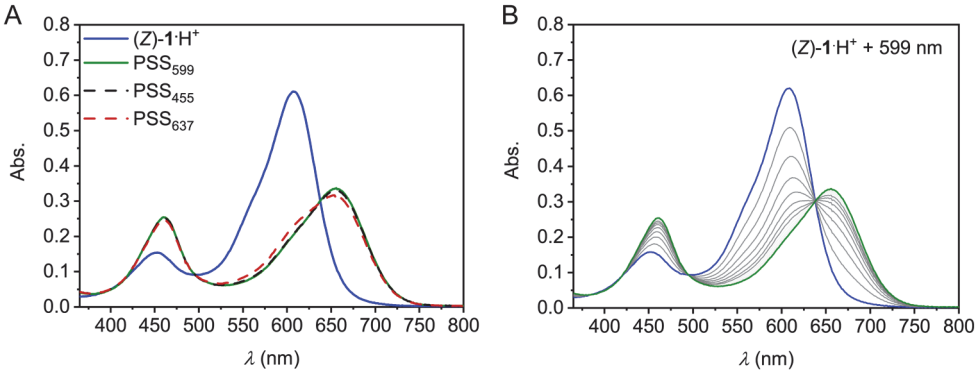

Figure 2. (A) UV-Vis spectral changes of (*Z*)-**1**·H$^+$ (10 μM in MeOH, 12 equiv. TFA, 293 K) upon sequential irradiation with 599 nm, 455 nm, and 637 nm light. (B) UV-Vis spectral changes measured in kinetic mode (60 s interval) during irradiation of (*Z*)-**1**·H$^+$ (10 μM in MeOH, 12 equivalents of TFA) with 599 nm; a clear isosbestic point at λ = 638 nm is maintained.

Next, this photoisomerization process was followed by ^{1}H NMR spectroscopy to quantify the *E*/*Z*-ratios at the PSS. Upon 599 nm irradiation of (*Z*)-**1**·H$^+$ in MeOD (containing 10 equiv. of TFA to ensure full protonation), a new set of signals appeared, while the original signals nearly disappeared (Figure 3, Figures E3-E4). The new signal set was assigned to the *E*-isomer and by relative signal integration the PSS_{599} *E*/*Z*-ratio was determined as 95:5. When the sample was subsequently irradiated with 455 nm and 637 nm light, only minor spectral changes were observed, and the PSS *E*/*Z*-ratios were found to be 91:9 and 86:14, respectively (Figure 3). This result confirms that, at the three different irradiation wavelengths used, the photoequilibrium lies towards the *E*-isomer. A similar observation was made previously for other heterocyclic hemi-(thio)indigo photoswitches able to form an intramolecular hydrogen bond. This high photoconversion has been ascribed to a reduction in quantum yield for isomerization from the intramolecularly hydrogen-bonded isomer.[43-46]

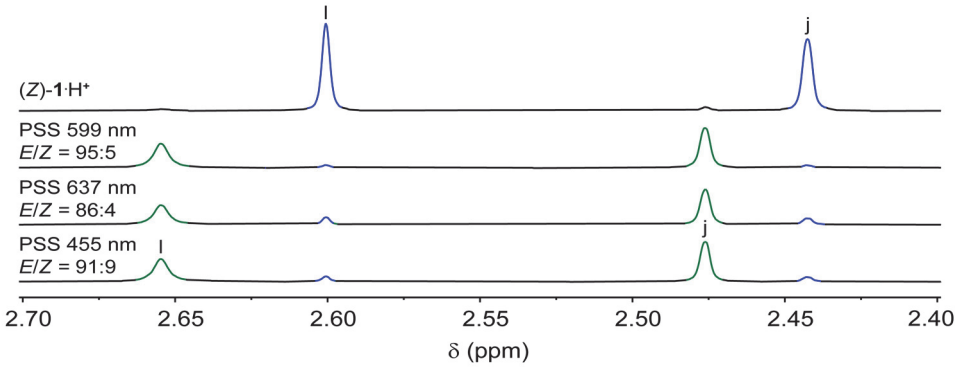

Figure 3. Aliphatic region in the ^{1}H NMR spectra (600 MHz, MeOD) of (*Z*)-**1**·H^{+} (0.15 mM, 10 equiv. TFA) upon sequential irradiation with 599 nm, 637 nm, and 455 nm light. The integrals of signals H**l** and H**j** were used to calculate the PSS ratios. For proton assignment, see Scheme 1A.

Then, binding of chloride was studied by ^{1}H NMR titrations in CD_2Cl_2/MeOD (95:5 v/v, 4 equiv. of TFA). For (*Z*)-**1**·H^{+}, addition of NBu_4Cl caused significant changes in chemical shifts, in particular of protons located close to the binding site, as a sign of chloride complexation (Figure 4).

These chemical shift changes were fitted to a 1:1 binding model with HypNMR,[53] affording an association constant of $K_a = (2.4 \pm 0.7) \times 10^4$ M^{-1} (Figure E5). A similar titration for the *E*-isomer, which was prepared by 599 nm irradiation of a solution of the *Z*-isomer, gave much smaller chemical shift changes (Figure E6). While these smaller changes could not be accurately fitted to a 1:1 binding model, they are an indication of weaker binding of chloride to the *E*-isomer compared to the *Z*-isomer. Negligible binding was observed in MeOD (with 2 equiv. TFA) for either isomer (Figures E7-E8).

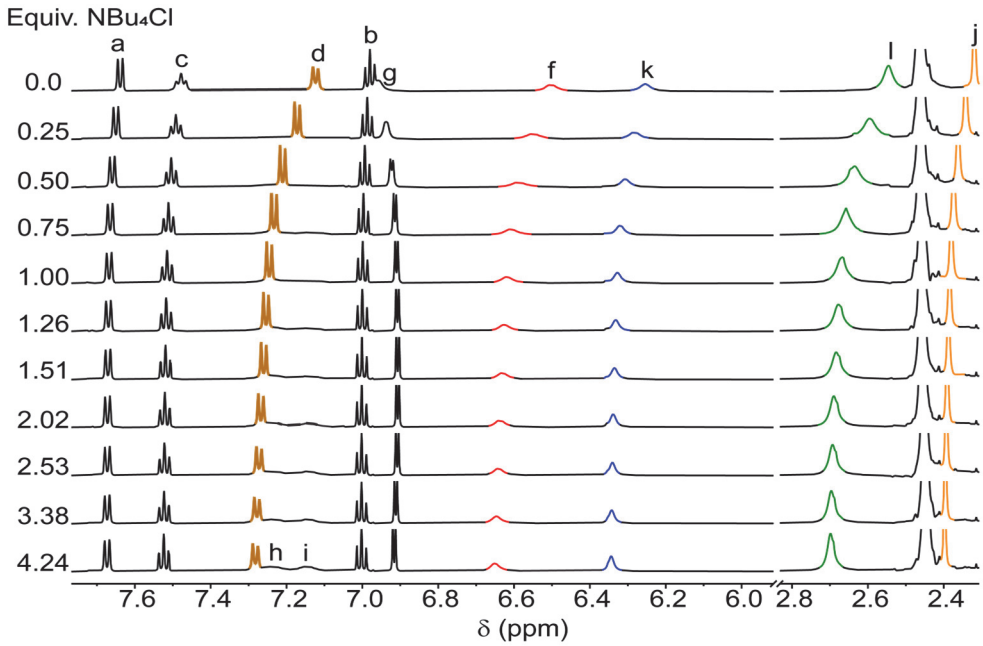

Figure 4. ^{1}H NMR spectra (600 MHz, CD_2Cl_2/MeOD 95:5 v/v) of (*Z*)-**1**·H^+ (1 mM, 4 equiv. of TFA) upon incremental addition of NBu_4Cl (100 mM).

5.5 Transport Activity

Subsequently, chloride transport activity and selectivity were evaluated using a cationophore-coupled ion-selective electrode (ISE) assay.[54] For this assay, POPC liposomes are prepared with an internal solution of KCl (300 mM) and an external solution of potassium gluconate (KGlu, 300 mM), both buffered to the desired pH value. The established chloride concentration gradient can only be dissipated by an anion transporter when coupled with an appropriate cationophore; otherwise buildup of charge or formation of a pH gradient impedes transport. The natural product valinomycin acts as an electrogenic potassium carrier and couples with an electrogenic chloride transporter to facilitate net KCl efflux. Conversely, monensin operates strictly through electroneutral K^+/H^+ exchange and couples with an electroneutral HCl transporter to give net KCl efflux. Comparing transport activity in presence of either cationophore therefore provides insight into the preferred mechanism (i.e. electrogenic Cl^- or electroneutral HCl transport, Figure 5A).

The ISE assay was first performed at pH 7.2 with (*Z*)-**1**·H^+ added to the liposome solution from MeOH (0.2 mol% with respect to POPC lipids). In the presence of valinomycin (0.1 mol%) negligible chloride efflux was observed, while in the presence of monensin (0.1 mol%) chloride transport was significant (Figure 5B). This difference confirms the anticipated

selectivity for the electroneutral HCl transport mechanism. That is, chloride is bound and transported across the bilayer by the protonated dipyrrin-derived hemi-indigo in a charge-neutral complex, while the compound diffuses back to the inner leaflet in deprotonated form.[24] In addition, a dose-response curve was constructed in the presence of monensin (Figure 5C). By fitting the transport data to the Hill equation, the half-maximal effective concentration was determined as EC_{50} = 0.076 mol% (see Table 1, Figure 6B and Figure E9), showing that the *Z*-isomer is a highly active transporter. When the same assay with (*Z*)-**1**·H^+ was performed at pH 5.5, higher transport activity was observed than at pH 7.2 (Figure 6A), whereas the strict selectivity for electroneutral HCl transport was retained (Figure E10). Hill analysis now gave a half-maximal effective concentration of EC_{50} = 0.011 mol% (Figure 6B and Figure E11), which is 7 times lower than the value determined at pH 7.2. The higher transport activity at a lower pH value supports that the protonated form of (*Z*)-**1** is the active chloride carrier, mechanistically similar to prodigiosin.[11-13]

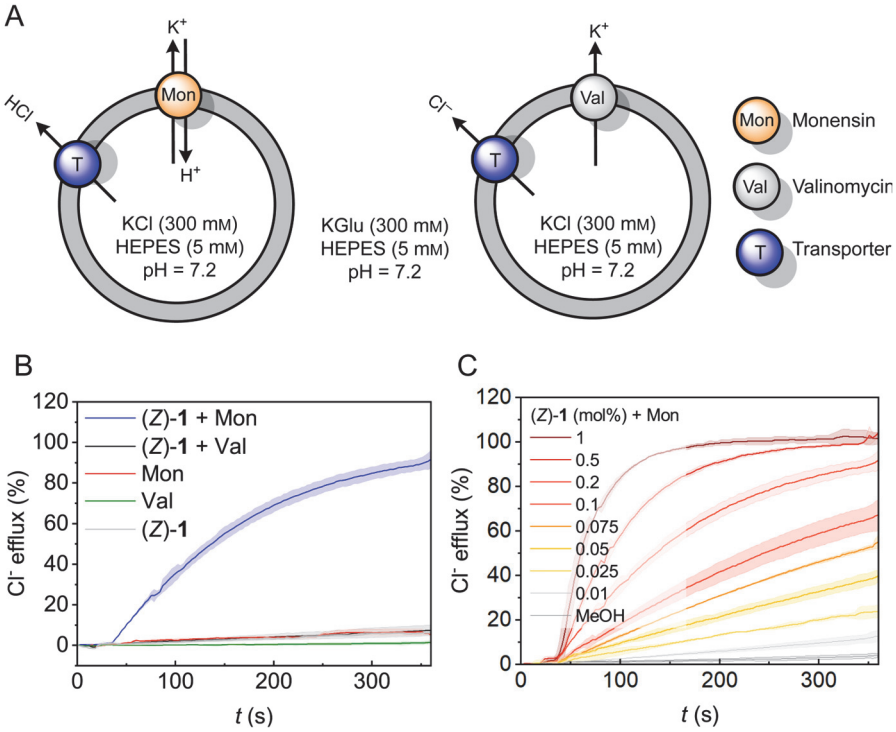

Figure 5. (A) Schematic representation of monensin (Mon) and valinomycin (Val) coupled ISE assay to determine selectivity for either electroneutral (HCl) or electrogenic (Cl^-) transport mechanisms. (B) Chloride efflux over time mediated by (Z)-**1** (0.2 mol% with respect to lipids) with 0.1 mol% of Monensin (Mon) or Valinomycin (Val). Blank experiments were also performed in which either MeOH (without transporter) or DMSO (without cationophore) was added. (C) Chloride efflux over time mediated by (Z)-**1** at varying loadings (mol% with respect to lipids) in the presence of monensin at pH 7.2

As no suitable chloride binding pocket is available in the *E*-isomer, we expected deactivation of transport by light irradiation. Therefore, the transport activity of the (E_{PSS})-mixture, obtained by irradiating a solution of (*Z*)-**1**·H$^+$ in MeOH with 599 nm light, was studied using the same ISE assay. To our delight, chloride efflux with (E_{PSS})-**1** was much lower than with (*Z*)-**1** at both pH values (Figure 6A). Hill analysis revealed a 16-fold and 14-fold decrease in HCl transport activity at pH 7.2 and 5.5, respectively (Table 1, Figure 6B and Figures E12-E15). The residual activity and pH sensitivity observed for (E_{PSS})-**1** is partially attributed to remaining *Z*-isomer.

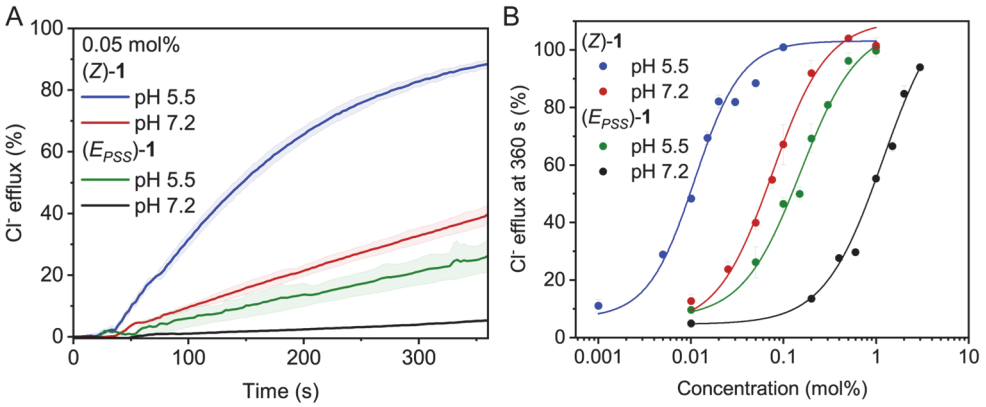

Figure 6. (A) Chloride efflux over time mediated by (*Z*)-**1** or (E_{PSS})-**1** (0.05 mol% with respect to lipids) in the presence of monensin at pH 7.2 and pH 5.5. (B) Hill plots of chloride efflux as a function of concentration for (*Z*)-**1** and photogenerated (E_{PSS})-**1** at pH 7.2 and pH 5.5.

Table 1. Comparison of EC_{50} values of (*Z*)-**1** and (E_{PSS})-**1** at pH 7.2 and pH 5.5.

pH	**EC_{50} (mol%)**[a] (*Z*)-**1**	**EC_{50} (mol%)**[a] (E_{PSS})-**1**	$F_{(E/Z)}$[b]
7.2	$(7.57 \pm 0.8) \times 10^{-2}$	1.18 ± 0.1	15.6
5.5	$(1.10 \pm 0.1) \times 10^{-2}$	$(1.53 \pm 0.2) \times 10^{-1}$	13.9

[a] EC_{50} defined as concentration (in mol% with respect to POPC lipids) required to reach 50% of the maximum activity at t = 360 s in the ISE assay as obtained by Hill analysis. [b] Factor decrease in transport activity by irradiation of (*Z*)-**1** to (E_{PSS})-**1** [$F = EC_{50(E)}/EC_{50(Z)}$].

To gain insight into the observed pH dependence of transport activity, the UV-Vis absorbance of both isomers of **1** in the POPC liposome at pH 5.5 and 7.2 was compared to that in MeOH solution in the presence of TFA and Et_3N (Figures E18-E19). In MeOH, the absorption of the protonated species is red-shifted with respect to that of the neutral species. Interestingly, the spectra recorded for the liposome samples at pH 5.5 and 7.2 closely resembled those taken in MeOH in the presence of TFA and Et_3N, respectively (Figures E18-E19). Additionally, various UV-Vis spectra were recorded for liposomes containing the *Z*-isomer in the pH range between 4 and 8, showing an inflection point around pH 6.7 (Figure E20). These results confirm that the transporter is in a protonated state at pH 5.5 and predominantly deprotonated at pH 7.2. The observed increase in transport activity at lower pH thus originates from facilitated protonation of the transporter.

Finally, we monitored the effect of *in situ* irradiation after incorporation of the compound into the bilayer, and prior to the addition of monensin (which initiates transport). Gratifyingly, the irradiated liposome samples showed strongly diminished chloride efflux both at pH 5.5 and 7.2 (Figure 7 and Figure E17). UV-Vis spectra of (*Z*)-**1** in the POPC bilayer were recorded before and after 599 nm irradiation to confirm that this decrease in transport activity is due to photo-induced *Z*-to-*E* isomerization. Indeed, irradiation resulted in a red-shift of the maximum and an overall decrease of the absorption at both pH 5.5. and 7.2 (Figures E21-E22), reminiscent of what was observed in MeOH solution in the presence of TFA and Et_3N (Figure E2). Importantly, the deactivating effect of *in-situ* irradiation verifies that the distinct activity of the two isomers is not due to an intrinsic difference in membrane deliverability.[37]

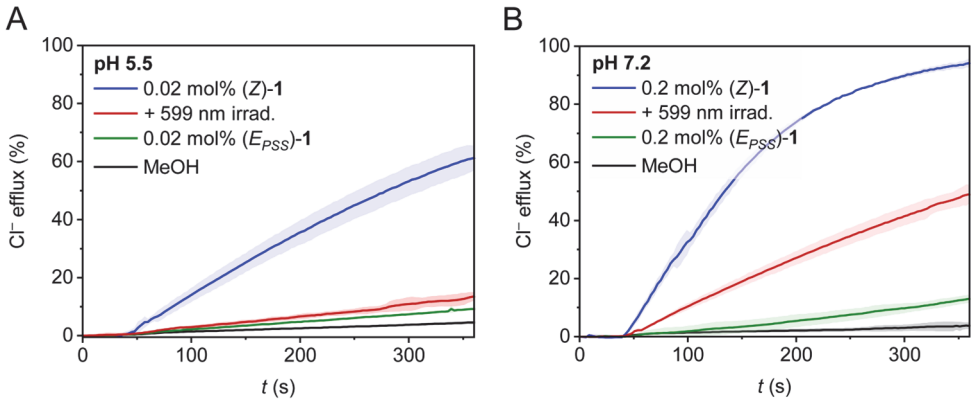

Figure 7. (A) Chloride efflux over time measured for (*Z*)-**1** at pH 5.5 added from MeOH (0.02 mol% with respect to lipids) with and without 599 nm irradiation of the liposome sample prior to addition of monensin. The traces are compared to that of (E_{PSS})-**1** pregenerated in and added from MeOH solution (0.02 mol% with respect to lipids) and an experiment in which only MeOH was added. (B) Chloride efflux over time measured for (*Z*)-**1** at pH 7.2 added from MeOH (0.2 mol% with respect to lipids) with and without 599 nm irradiation of the liposome sample prior to addition of monensin. The traces are compared to that of (E_{PSS})-**1** pregenerated in and added from MeOH solution (0.2 mol% with respect to lipids) and an experiment in which only MeOH was added.

5.6 Conclusion

In summary, we have developed a pH and red-light responsive prodigiosin-like transporter by dipyrrin functionalization of hemi-indigo. The *Z*-isomer strongly binds chloride when protonated and facilitates strictly electroneutral HCl symport across the POPC bilayer membrane. Importantly, it is more active in an acidic environment (at pH 5.5 compared to pH 7.2) and can be deactivated by visible-light irradiation. That is, irradiation gives high conversion to the intramolecularly hydrogen-bonded, less active *E*-isomer. Such efficient deactivation of transport by visible light is unprecedented and will be useful to reduce undesired cytotoxicity in healthy tissue and/or after excretion into the environment.

5.7 Contributions

N. Duindam, J. E. Bos, and S. J. Wezenberg conceived the project. N. Duindam carried out the experimental work. F. van Nifterik assisted in the initial synthetic work, and J. E. Bos performed exploratory transport experiments. S. J. Wezenberg guided the project.

5.8 Experimental Section

Pyrrole-derived hemi-indigo (*Z*)-**S1** was synthesized according to a procedure reported in the literature.[47] All other chemicals were commercially available and were used without further purification. Flash chromatography (FC) was performed using SiO_2 (60 M, 0.04-0.063 mm) or C_{18}-functionalized SiO_2 (5.4g, high-efficiency spherical C18, 15um, 100A,C 17%, end-capped, 320m^2/g) purchased from Screening Devices BV. Thin-layer chromatography (TLC) was carried out on aluminum sheets coated with silica (60 Å, UV254 indicator) or coated with C_{18}-functionalized SiO_2 (0.15 mm C_{18} silica gel with UV254 indicator, Macherey Nagel Alugram Plates). Compounds were visualized with UV light (254 nm or 365 nm). ^{1}H, ^{19}F, and ^{13}C NMR spectra were recorded on Bruker AV 400 MHz, Bruker 500 MHz Ultra Shield, Bruker AV-III 600 MHz, and Bruker AV-III-HD 850 MHz instruments at 298 K unless indicated otherwise. Chemical shifts (δ) are denoted in parts per million (ppm) relative to residual protiated solvent (CD_2Cl_2: for ^{1}H detection, δ = 5.32 ppm; for ^{13}C detection, δ = 53.84 ppm, MeOD: for ^{1}H detection, δ = 3.31 ppm; for ^{13}C detection, δ = 49.00 ppm). The splitting pattern of peaks is designated as follows: s (singlet), d (doublet), t (triplet), q (quartet), p (quintet), h (septet), m (multiplet), br (broad). High-resolution mass spectrometry (ESI-MS) was performed on a Thermo Scientific Q Exactive HF spectrometer with ESI ionization. IR spectra were recorded on a Perkin Elmer Spectrum Two FT-IR spectrometer. The intensity of bands (ν = cm^{-1}) is assigned as follows: s (strong), m (medium), w (weak), very w (very weak), br (broad), and sh (shoulder). Melting points were determined with a Büchi M560 apparatus. UV-Vis spectra were recorded on an Agilent Cary 8454 spectrometer or a Perkin Elmer Lambda 465 spectrometer using 1 cm or 1 mm quartz cuvettes. Irradiation of UV-Vis and NMR samples was carried out using LEDs purchased from Thorlabs: M455F3 (17 mW minimal LED output, 1000 mA, peak wavelength = 455 nm, FWHM = 14 nm), M590L4 (230 mW minimal LED output power, 1000 mA, peak wavelength = 599 nm, FWHM = 15 nm), M625L4 (700 mW minimal LED output power, 1000 mA, peak wavelength = 637 nm, FWHM = 17 nm). In this work, the peak wavelength (maximum emission intensity) is referred to, rather than following convention by Thorlabs of taking the nominal wavelength (defined as the wavelength at which the LED appears brightest to the human eye).

General procedure for the MacDonald-type condensation:

The reagent to mediate the condensation (see Table E1) was added to 3,5-Dimethyl-1*H*-pyrrole-2-carbaldehyde (**S2**) and (*Z*)-**S1** (20 mg, 0.095 mmol) in dry and degassed MeOH (4 mL) under argon atmosphere. After the indicated reaction time, the reaction mixture was concentrated *in vacuo* and the conversion was determined by ^{1}H NMR spectroscopy. In case of significant conversion, the desired product was purified by FC (C_{18} SiO_2; CH_3CN:H_2O 2:8 to 8:2 with 0.1 v% TFA) and freeze-dried to obtain the TFA salt. ^{1}H NMR spectral characterization matched that of the product obtained by the improved method as described below.

Equiv. S2	Reagent (equiv.)	Solvent	Temp.	Time	% (*Z*)-1
1.0	HBr[a] (5.0)	MeOH	20 °C	12 h	trace
1.0	*p*TsOH (5.0)	MeOH	20 °C	30 min	trace
1.6	HCl[b] (10.0)	MeOH	20 °C	3 h	2%[d]
0.5	HCl[b] (10.0)	MeOH	20 °C	3 h	2%[d]
1.6	TFA (5.0)	MeOH	20 °C	3 h	4%[d]
1.6[c]	TFA (5.0)	MeOH	20 °C	3 h	3%[d]
1.6	$InCl_3$ (0.2)	MeOH	20 °C	48 h	None

Table E1. Used conditions to mediate the condensation reaction of (*Z*)-**S1** with aldehyde **S2**. [a] Added as a 33 wt% solution in acetic acid. [b] Added as a 0.5 M solution in MeOH. [c] **S2** was added as a MeOH solution (2 mL) over a period of 1 h to a premixed solution of (*Z*)-**S1** and TFA (2 mL MeOH). [d] Isolated yields (after purification by FC) are provided.

Dipyrrin-derived hemi-indigo (*Z*)-1·TFA

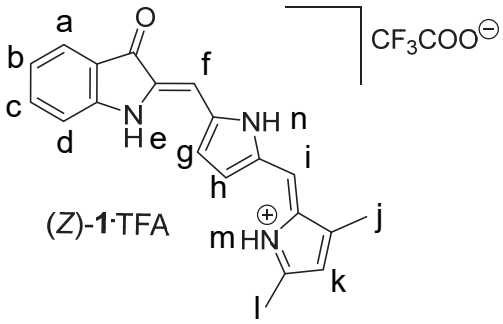

3,5-Dimethyl-1*H*-pyrrole-2-carbaldehyde (21 mg, 0.17 mmol) and (*Z*)-**S1** (30 mg, 0.14 mmol) were dissolved in dried and degassed CH_2Cl_2 (3 mL) under argon atmosphere. The stirring solution was cooled to 0 °C and $POCl_3$ (36 µL, 0.43 mmol) was added dropwise over a period of 1 minute. The mixture was stirred at 0 °C for an additional 5 minutes, after which it was allowed to warm to rt and stirred for a further 15 minutes. The mixture was then treated with MeOH (1 mL) and poured into petroleum ether (60 mL) and, while cooled at 4 °C, a fine precipitate formed after 30 minutes. The supernatant was removed and the precipitate was redissolved in MeOH (1 mL) containing TFA (20 µL). Addition to petroleum ether (60 mL) again led to precipitation and after removal of the supernatant, the precipitate was dissolved in $CHCl_3$ (5 mL) and precipitated by addition of petroleum ether (10 mL, performed twice). The precipitate was then dispersed in MilliQ water containing TFA (0.1 v%) and lyophilized to afford the TFA salt of (*Z*)-**1** as a dark purple solid (38 mg, 62%).

Note: In the ^{13}C NMR spectrum acquired at 298 K in MeOD three carbon signals are missing, *i.e.* a quaternary carbon signal and two pyrrolic carbon signals. These signals most likely broaden into the baseline due to rotamer interconversion. Therefore, ^{1}H and ^{13}C NMR spectra were additionally recorded in CD_2Cl_2 in presence of NBu_4Cl (2 equiv.) and TFA (2 equiv.) at 263 K. Under these conditions the rotamer-induced peak broadening is reduced, and all ^{13}C signals are observed.

R_f = 0.12 (SiO_2-C_{18}; CH_3CN/H_2O 1:1 with 0.1 v% TFA); m.p. > 300 °C decomp; ^{1}H NMR (850 MHz, MeOD, assignment based on 2D COSY and NOESY spectra) δ = 7.77 (s, 1H; H**h**), 7.65 (d, J = 7.5 Hz, 1H; H**a**), 7.58 (s, 1H; H**i**), 7.56 (ddd, J = 8.3, 7.2, 1.3 Hz, 1H; H**c**), 7.36 (d, J = 4.6 Hz, 1H; H**g**), 7.16 (d, J = 8.0 Hz, 1H; H**d**), 7.02 (td, J = 7.4, 0.8 Hz, 1H; H**b**), 6.62 (s, 1H; H**f**), 6.51 (s, 1H; H**k**), 2.59 (s, 3H; H**l**), 2.42 (s, 3H; H**j**); ^{1}H NMR (600 MHz, CD_2Cl_2, 2 equiv.

TFA and 2 equiv. NBu_4Cl, 263 K) δ 14.09 (s, 1H; H**m**), 12.72 (s, 1H; H**n**), 11.07 (s, 1H; H**e**), 7.60 (d, *J* = 7.5 Hz, 1H; H**a**), 7.43 (t, *J* = 7.6 Hz, 1H; H**c**), 7.24 (d, *J* = 8.0 Hz, 1H; H**d**), 7.15 (s, 1H; H**h**), 7.01 (s, 1H; H**i**), 6.96 – 6.91 (m, 2H; H**b** and H**g**), 6.55 (s, 1H; H**f**), 6.28 (s, 1H; H**k**), 2.66 (s, 3H; H**l**), 2.32 (s, 3H; H**j**); ^{13}C NMR (214 MHz, MeOD) δ = 188.1, 161.9, 154.8, 151.7, 138.8, 138.2, 133.2, 132.2, 125.7, 125.0, 122.4, 121.4, 121.0, 113.6, 96.8, 14.7, 12.1; ^{13}C NMR (151 MHz, CD_2Cl_2, 2 equiv. NBu_4Cl and TFA, 263 K, assignment based on 2D COSY and NOESY spectra) δ 187.1, 159.6, 153.4, 149.0, 147.1, 136.6, 136.1, 134.8, 131.3, 129.8, 124.7, 122.2, 121.5, 121.1, 120.2, 119.4, 112.9, 96.1, 14.9, 12.4; ^{19}F NMR (376 MHz, MeOD) δ –76.6; IR (ATR) ν = 3225 (br, w), 3128 (w), 3001 (very w), 1687 (m, sh), 1671 (m), 1614 (s), 1560 (s, sh), 1543 (m), 1517.8 (w), 1482 (w), 1466 (w, sh), 1424 (very w), 1383 (m), 1324 (very w), 1313 (very w), 1285 (m), 1265 (w), 1246 (very w), 1193 (s), 1176 (m), 1127 (s), 1076 (m), 964 (m), 954 (m, sh), 941 (m, sh), 890 (very w), 833 (m), 800 (m), 778 (w), 756 (m), 720 (m), 710 (w, sh), 655 (m), 617 (w); UV-Vis (MeOH): λ_{max} (ε) = 452 nm (1.5×10^4 M^{-1} cm^{-1}), 608 nm (6.1×10^4 M^{-1} cm^{-1}); HRMS (ESI) *m/z:* 316.1444 ($[M+H]^+$, calcd for $C_{20}H_{18}N_3O^+$: 316.1444); elemental analysis calcd (%) for [$C_{20}H_{18}N_3O^+$ + CF_3COO^-]: 61.54 %, H: 4.23%, N: 9.79%. C: 61.02 %, H: 4.44%, N: 9.63%.

UV-Vis photoisomerization studies

Solutions of the *Z*-isomers were prepared in dried and degassed spectroscopic grade acetonitrile at a suitable concentration (Abs < 1.0) in a 1 cm quartz cuvette. Subsequently, TFA and Et_3N were added in these studies such that no further spectral changes were observed after the addition of more equivalents. The samples measured in the presence of base were measured at 273 K, as the neutral form of **1** is expected to equilibrate between multiple tautomeric forms. Indeed, spectral changes were observed over time that are best accounted for by tautomerization. The given spectra thus belong to isomer mixtures, but identification of these mixtures is beyond the scope of this work. In the protonated form, which we study herein, these tautomeric forms are degenerate.

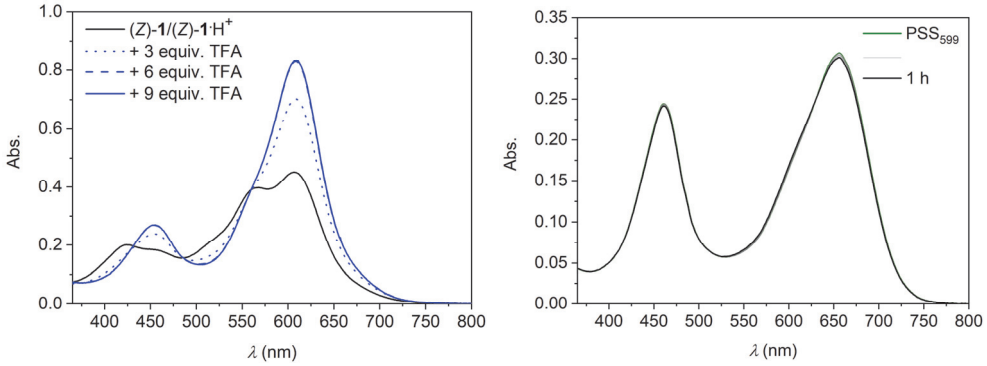

Figure E1. (left) UV-Vis spectral changes of a solution of as-isolated (*Z*)-**1**·TFA (15 μM in MeOH) upon addition of more TFA (0.05 M in MeOH). (right) UV-Vis spectra of (E_{PSS})-**1**·H^+ (10 μM in MeOH, 12 equiv. of TFA) in the dark (600 s interval); DAbs. (at 655 nm) ≤ 2% after 1 h, highlighting the thermal stability.

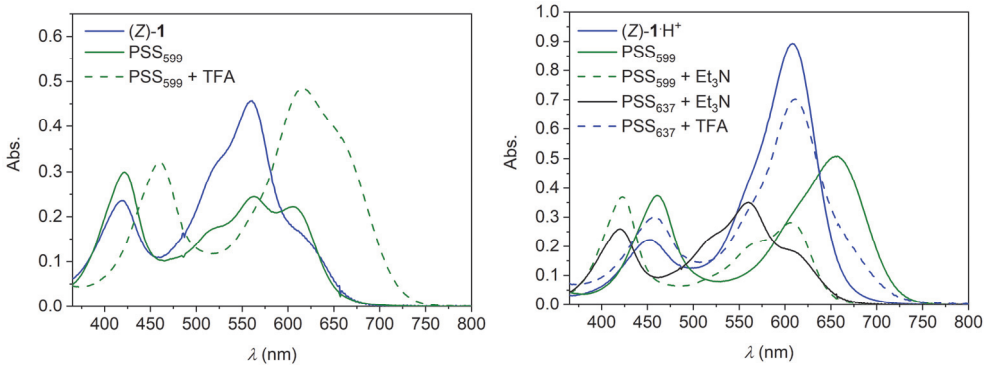

Figure E2. (left) UV-Vis spectral changes of (*Z*)-**1** (15 μM in MeOH, 3 equiv. Et_3N, 273 K) upon irradiation with 599 nm light until the PSS was reached and after reacidification with TFA (20 equiv.). (right) UV-Vis spectral changes of (*Z*)-**1**·H^+ (15 μM in MeOH, 3 equiv. TFA, 273 K) upon irradiation with 599 nm light until the PSS was reached and after basification with Et_3N (20 equiv.). Subsequently, the basified PSS_{599} was irradiated with 637 nm light until a new PSS was reached, after which the sample was acidified with TFA (40 equiv.).

^{1}H NMR photoisomerization studies

A solution of (*Z*)-**1**·H$^+$ (0.15 mM, MeOD) was prepared, and additional TFA (10 equiv.) was added to ensure quantitative protonation. The solution was transferred to a NMR tube, which was sealed with parafilm, and irradiated with 599 nm, 637 nm, and 455 nm until the photostationary state was reached. Signal integration was used to determine the PSS ratio.

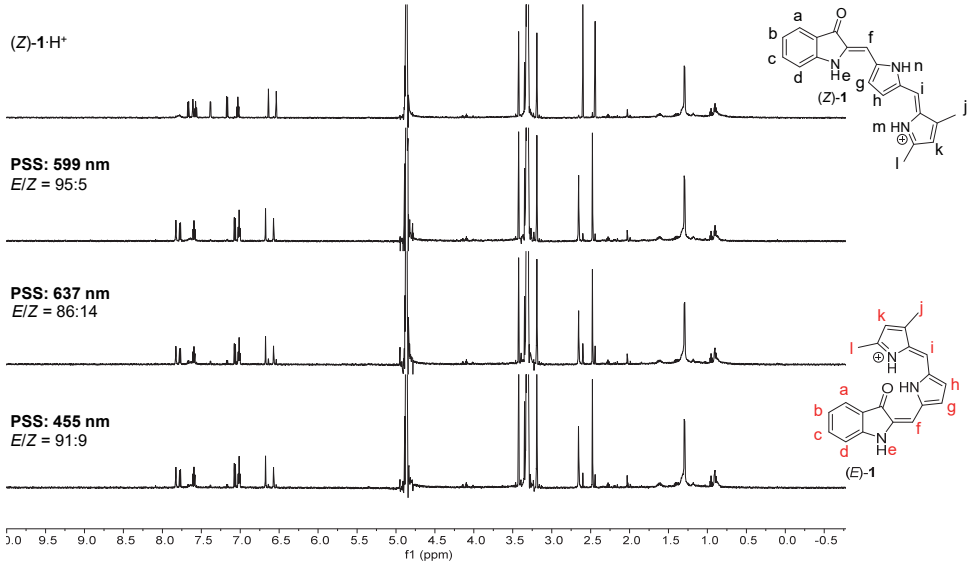

Figure E3. ^{1}H NMR spectra (600 MHz, MeOD) of (*Z*)-**1**·H$^+$ (0.15 mM, 10 equiv. TFA) upon sequential irradiation with 599 nm, 637 nm, and 455 nm light. The integrals of signals H**l** and H**j** were used to calculate the PSS ratios. For signal assignments, see the amplification of the aromatic and aliphatic region in Figure E4 and Figure 3, respectively.

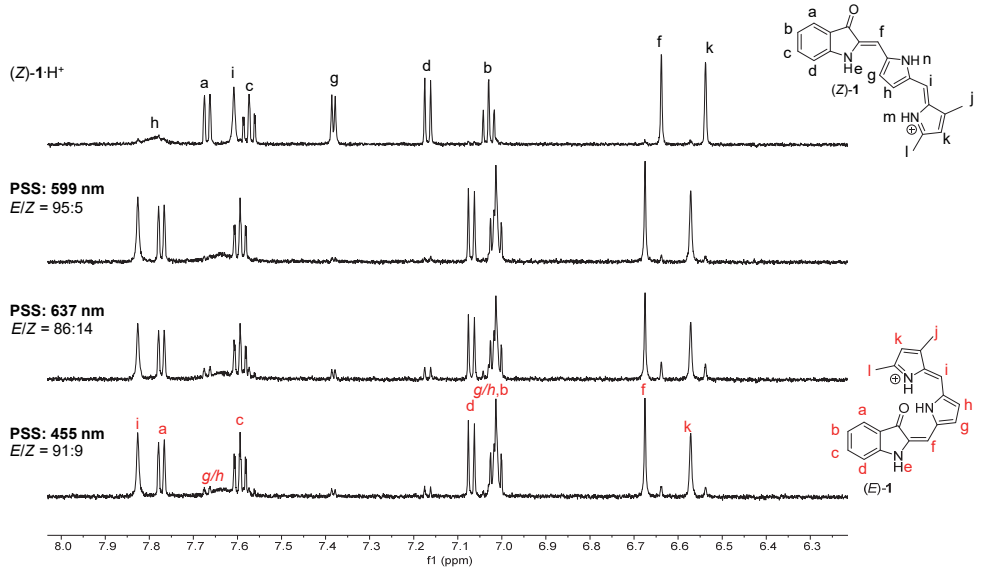

Figure E4. Aromatic region in the ^{1}H NMR spectra (600 MHz, MeOD) of (*Z*)-**1**·H$^+$ (0.15 mM, 10 equiv. TFA) upon sequential irradiation with 599 nm, 637 nm and 455 nm light. The integrals of signals H**l** and H**j** were used to calculate the PSS ratios.

^{1}H NMR titration studies

Prior to titration experiments 10 mg aliquots of (Z)-**1**·TFA were additionally purified using FC (C_{18} SiO_2; CH_3CN:H_2O 2:8 to 8:2 with 0.1v% TFA) and freeze-dried. First, the as-isolated (*Z*)-**1**·TFA was dissolved in either MeOD or CD_2Cl_2/MeOD (95:5 v/v) to give a 1 mM solution. The (*E*)-isomer was generated by irradiation of the (*Z*)-isomer in MeOD (1 mM) with 599 nm light. This solution was used as is or concentrated and redissolved in CD_2Cl_2/MeOD (95:5 v/v) to a concentration of 1 mM. Separate solutions of NBu_4Cl (100 mM or 1.0 M) were prepared in the same solvent (mixture). The titrations were performed in presence of additional trifluoracetic acid [2 equiv. TFA in MeOD and 4 equiv. TFA in CD_2Cl_2/MeOD (95:5 v/v)] to ensure full protonation. Small aliquots of the guest solution were added to the receptor solution, and after each addition a ^{1}H NMR spectrum was recorded. The changes in chemical shift were fitted assuming 1:1 binding equilibrium using HypNMR.[53]

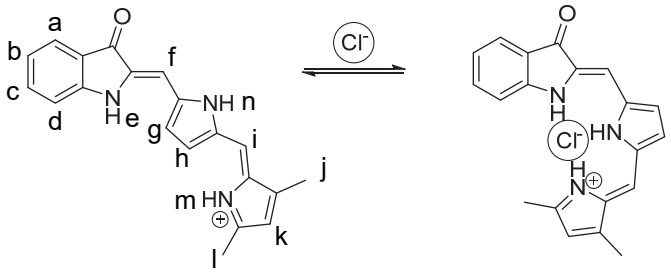

Scheme E1. Scheme of binding equilibrium including the lettering assignment of (*Z*)-**1**·H$^+$.

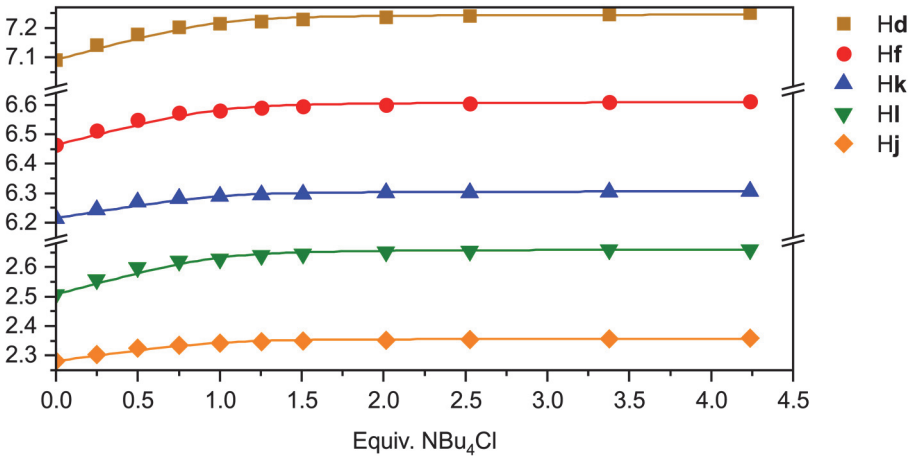

Figure E5. Titration curves for the addition of NBu_4Cl to (*Z*)-**1**·H$^+$ and data fits obtained by simultaneous analysis of the indicated proton signals using HypNMR^2 and a 1:1 binding model; $\log(K_a) = 4.37 \pm 0.127$, or $K_a = (2.4 \pm 0.7) \times 10^4$ M^{-1}.

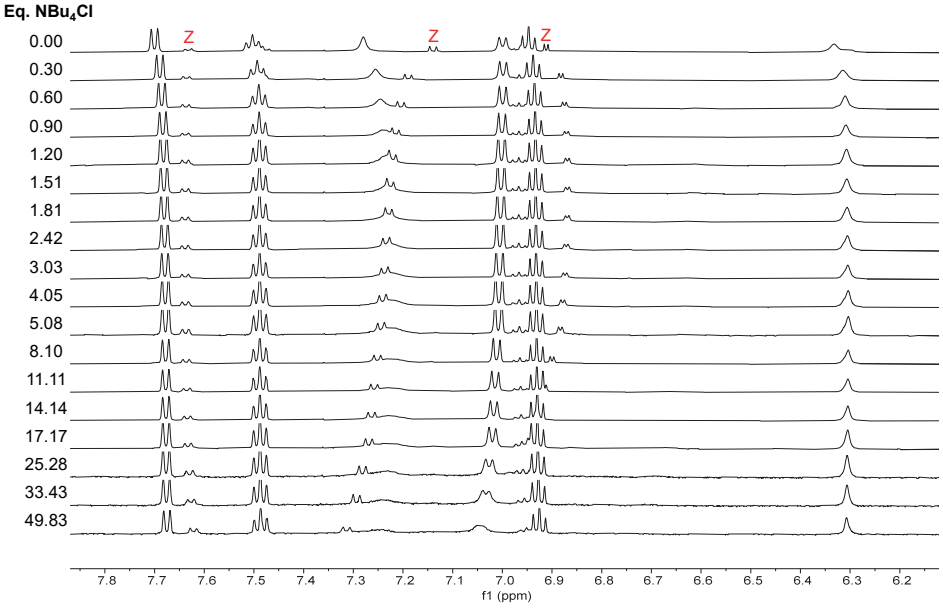

Figure E6. ^{1}H NMR spectra (600 MHz, CD_2Cl_2/MeOD 95:5 v/v) of (E_{PSS})-**1**·H$^+$ (1 mM, 4 equiv. of TFA) upon incremental addition of NBu_4Cl (100 mM). By relative ^{1}H NMR signal integration, an *E*/*Z* ratio of 16:84 was determined at the start of the titration.

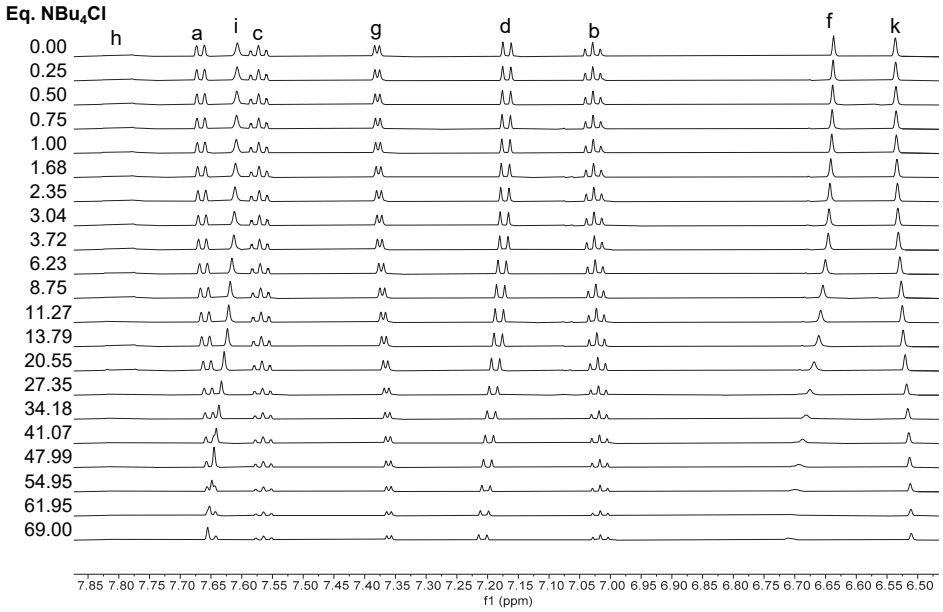

Figure E7. ^{1}H NMR spectra (600 MHz, MeOD) of (*Z*)-**1**·H$^+$ (1 mM, 2 equiv. TFA) upon incremental addition of NBu_4Cl (100 mM and 1.0 M).

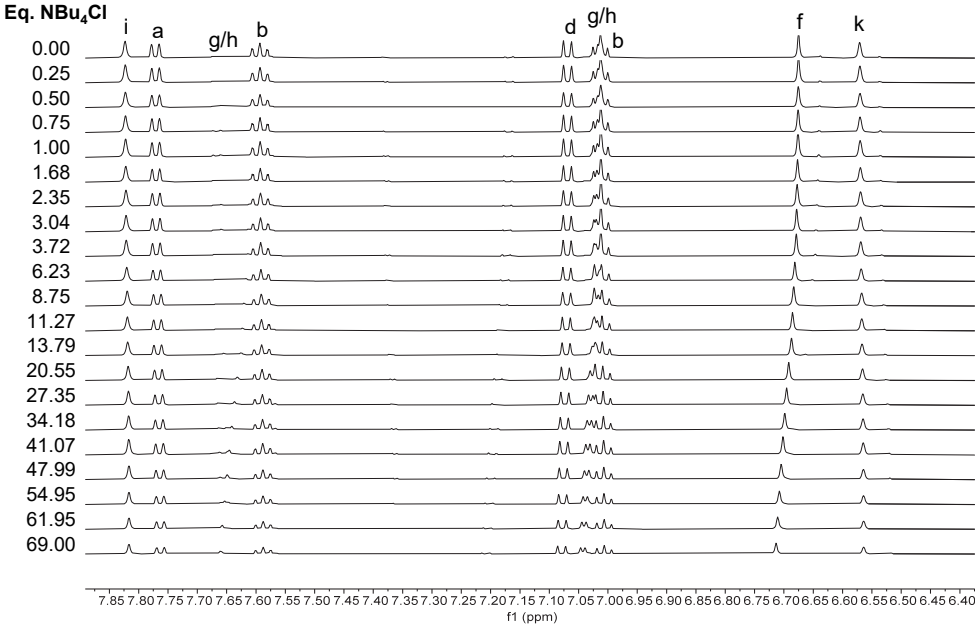

Figure E8. ^{1}H NMR spectra (600 MHz, MeOD) of (E_{PSS})-**1**·H^{+} (1 mM, 2 equiv. TFA) upon incremental addition of NBu_4Cl (100 mM and 1.0 M).

Cationophore-coupled ISE assays

The ISE transport assay was performed according to the procedure previously described by the group of Gale.[16] A lipid film was prepared by evaporating a solution of POPC in $CHCl_3$ in a round-bottom flask, followed by drying under high vacuum for at least 12 h. The lipid film was hydrated with an aqueous solution of 300 mM KCl buffered with either HEPES (pH 7.2, 5 mM) or MES (pH 5.5, 5 mM) and the resulting suspension was vortexed. Subsequently, the suspension was subjected to 9 freeze-thaw cycles, by freezing the sample in liquid nitrogen and thawing in a water bath (45 °C). The sample was allowed to equilibrate for 30 minutes, after which it was extruded 25 times through a 200 nm polycarbonate membrane to obtain unilamellar vesicles. An Illustra NAP™-25 Sephadex® G-25 column was equilibrated with an aqueous solution of 300 mM KGlu buffered with either HEPES (pH 7.2, 5 mM) or MES (pH 5.5, 5 mM) and the liposome suspension was eluted on this column using the aqueous KGlu solution to exchange KCl for KGlu.

Prior to the measurement the ISE chloride selective electrode was calibrated using a series of solutions with a known chloride concentration: 0.159 mM, 0.318 mM, 0.625 mM, 1.25 mM, 2.50 mM, 5.00 mM, and 10.0 mM. By fitting the calibration data to equation E**1** constants *a* and *b* could be obtained.

$$E\ (\mathrm{mV}) = \mathrm{a} + \mathrm{b}\log[\mathrm{Cl}] \qquad \text{(Eq. E1)}$$

Subsequently, a measured value of *E* (mV) could be converted into [Cl] by using equation E**2**.

$$[\mathrm{Cl}] = 10^{\left(\frac{E-\mathrm{a}}{\mathrm{b}}\right)} \qquad \text{(Eq. E2)}$$

For each measurement the liposome solution was diluted to 1.0 mM in the aqueous solution of 300 mM KGlu buffered with either HEPES (pH 7.2, 5 mM) or MES (pH 5.5, 5 mM) in a glass vial. Chloride efflux was measured over a time course of 8 minutes, with a data interval of 3 s.

At t = 15 s either MeOH (blank) or a solution of the transporter in MeOH was added, and after t = 30 s DMSO (blank) or a DMSO solution of either monensin or valinomycin (0.1 mol%, 5 µL) was added to initiate transport. After 6 minutes (t = 360 s) the liposomes were lysed with Triton-X (50 µL, 11 wt% in H_2O/DMSO 7:1 v/v) and after t = 480 s the final reading was taken.

The obtained changes in chloride concentration were normalized to give the percentage of chloride efflux using equation E**3**. All experiments were performed in duplicate.

$$\% \text{ Cl} = \frac{[\text{Cl}]_t - [\text{Cl}]_0}{[\text{Cl}]_{360} - [\text{Cl}]_0} \times 100 \qquad \text{(Eq. E3)}$$

Note: Prior to transport studies, 10 mg aliquots were additionally purified using FC (C_{18} SiO_2; CH_3CN:H_2O 2:8 to 8:2 with 0.1v% TFA). The assay was performed in the dark, to avoid photoisomerization during the execution of the assay. For the transport assays with the (*E*)-isomer, (*E*$_{PSS}$)-**1**·H^+ was generated photochemically by irradiating a solution of (*Z*)-**1**·TFA in MeOH (1 mM) with 599 nm light (from here on referred to as (*E*$_{PSS}$)-**1**). Photoisomerization was followed by UV-Vis spectroscopy to ensure the PSS was reached.

EC_{50} determination of (*Z*)-1 at pH 7.2

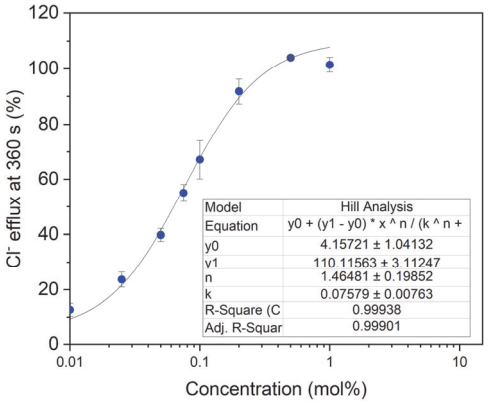

Figure E9. Chloride efflux at *t* = 360 s in the monensin-coupled ISE assay plotted versus concentration and fit to the Hill equation. The same data is shown in Figure 6B without details of the fit; $EC_{50} = 7.6 \times 10^{-2}$ mol% (with respect to lipids).

Selectivity assay and EC_{50} determination of (*Z*)-1 at pH 5.5

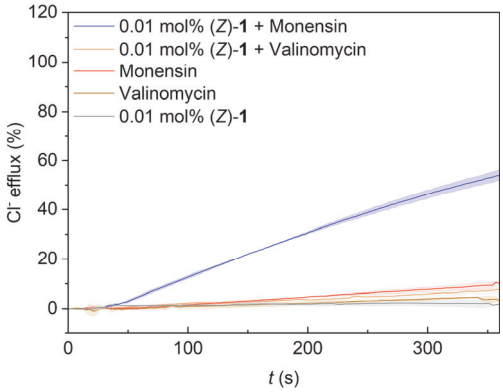

Figure E10. Chloride efflux plotted versus time as measured by a chloride selective electrode in the cationophore-coupled assay. The transporter was added from MeOH (1.0 mM stock solution) to the aqueous liposome solution (1.0 mM POPC, 300 mM internal KCl, 300 mM external KGlu buffered with MES to pH 5.5) at t = 15 s, followed by monensin (0.1 mol%) or valinomycin (0.1 mol%) from DMSO at t = 30 s, and an aqueous Triton-X solution at t = 360 s. Blank experiments were also performed in which either MeOH (without transporter) or DMSO (without cationophore) was added.

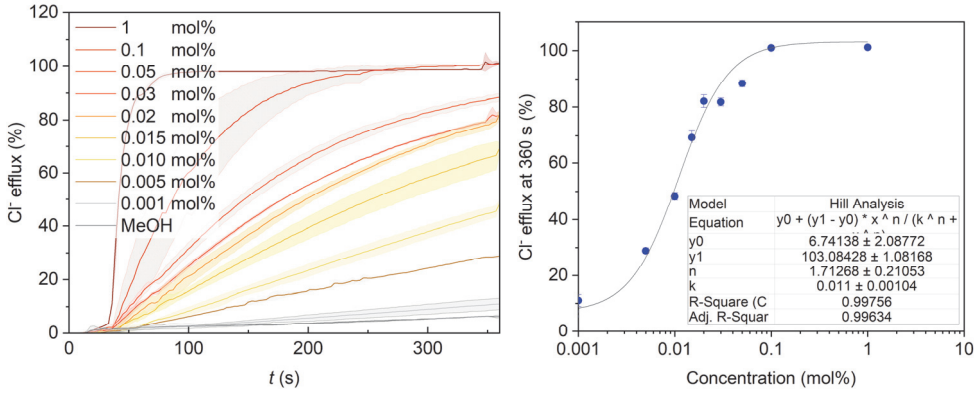

Figure E11. (Left) Chloride efflux plotted versus time as measured by a chloride selective electrode in the monensin-coupled assay. The transporter was added from MeOH (1.0 mM stock solution) to the aqueous liposome solution (1.0 mM POPC, 300 mM internal KCl, 300 mM external KGlu buffered with MES to pH 5.5) at t = 15 s, followed by monensin (0.1 mol%) from DMSO at t = 30 s, and an aqueous Triton-X solution at t = 360 s. Blank experiments were also performed in which MeOH (without transporter) was added. (right) Chloride efflux at t = 360 s in the monensin-coupled ISE assay plotted versus concentration and fit to the Hill equation. The same data is shown in Figure 6B without details of the fit; $EC_{50} = 1.1 \times 10^{-2}$ mol% (with respect to lipids).

Selectivity assay and EC_{50} determination of (E_{PSS})-1 at pH 7.2

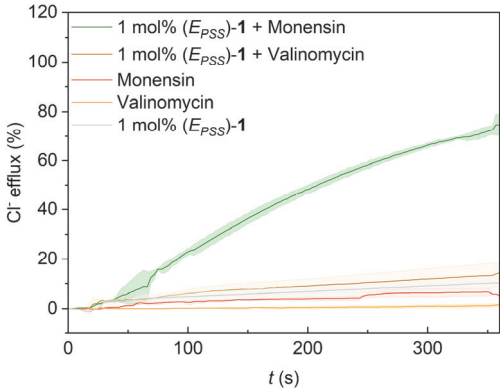

Figure E12. Chloride efflux plotted versus time as measured by a chloride selective electrode in the cationophore-coupled assay. The transporter was added from MeOH (1.0 mM stock solution) to the aqueous liposome solution (1.0 mM POPC, 300 mM internal KCl, 300 mM external KGlu buffered with HEPES to pH 7.2) at t = 15 s, followed by monensin (0.1 mol%) or valinomycin (0.1 mol%) from DMSO at t = 30 s, and an aqueous Triton-X solution at t = 360 s. Blank experiments were also performed in which either MeOH (without transporter) or DMSO (without cationophore) was added.

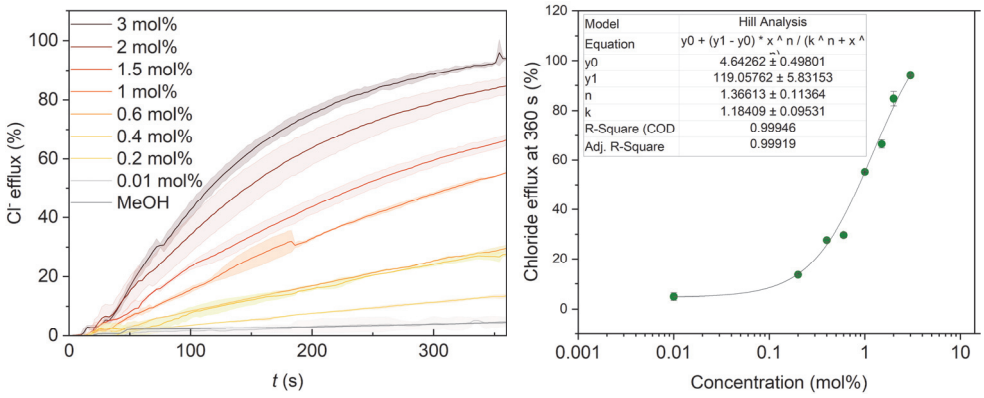

Figure E13. (Left) Chloride efflux plotted versus time as measured by a chloride selective electrode in the monensin-coupled assay. The transporter was added from MeOH (1.0 mM stock solution) to the aqueous liposome solution (1.0 mM POPC, 300 mM internal KCl, 300 mM external KGlu buffered with HEPES to pH 7.2) at t = 15 s, followed by monensin (0.1 mol%) from DMSO at t = 30 s, and an aqueous Triton-X solution at t = 360 s. Blank experiments were also performed in which MeOH (without transporter) was added. (Right) Chloride efflux at t = 360 s in the monensin-coupled ISE assay plotted versus concentration and fit to the Hill equation. The same data is shown in Figure 6B without details of the fit; EC_{50} = 1.18 mol% (with respect to lipids).

Selectivity assay and EC_{50} determination of (E_{PSS})-1 at pH 5.5

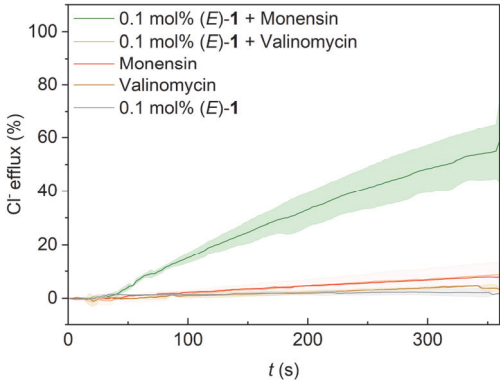

Figure E14. Chloride efflux plotted versus time as measured by a chloride selective electrode in the cationophore-coupled assay. The transporter was added from MeOH (1.0 mM stock solution) to the aqueous liposome solution (1.0 mM POPC, 300 mM internal KCl, 300 mM external KGlu buffered with MES to pH 5.5) at t = 15 s, followed by monensin (0.1 mol%) or valinomycin (0.1 mol%) from DMSO at t = 30 s, and an aqueous Triton-X solution at t = 360 s. Blank experiments were also performed in which either MeOH (without transporter) or DMSO (without cationophore) was added.

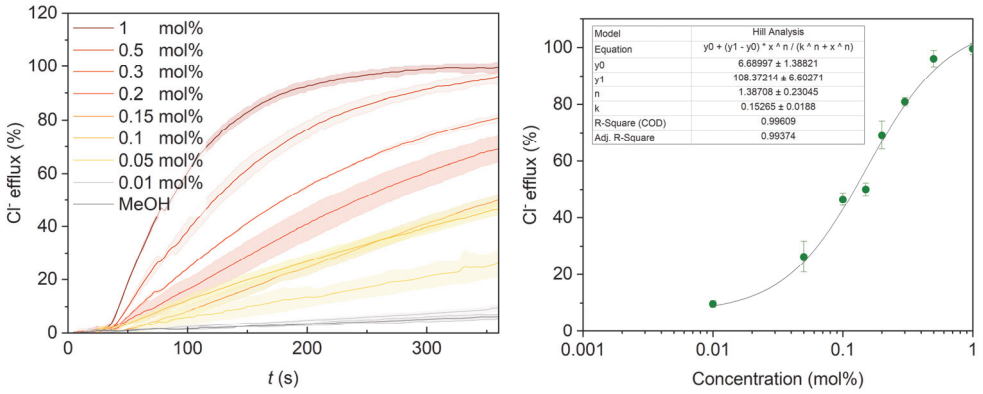

Figure E15. (Top) Chloride efflux plotted versus time as measured by a chloride selective electrode in the monensin-coupled assay. The transporter was added from MeOH (1.0 mM stock solution) to the aqueous liposome solution (1.0 mM POPC, 300 mM internal KCl, 300 mM external KGlu buffered with MES to pH 5.5) at t = 15 s, followed by monensin (0.1 mol%) from DMSO at t = 30 s, and an aqueous Triton-X solution at t = 360 s. Blank experiments were also performed in which MeOH (without transporter) was added. (Bottom) Chloride efflux at t = 360 s in the monensin-coupled ISE assay plotted versus concentration and fit to the Hill equation. The same data is shown in Figure 6B without details of the fit; $EC_{50} = 1.5 \times 10^{-1}$ mol% (with respect to lipids).

Comparison of (*Z*)-1 and (E_{PSS})-1

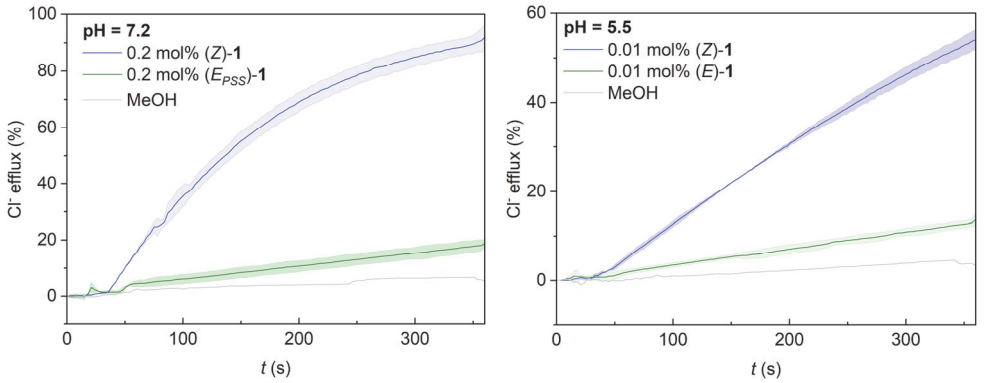

Figure E16. Chloride efflux plotted versus time as measured by a chloride selective electrode in the monensin-coupled assay. The transporters were added from MeOH (1.0 mM stock solution) to the aqueous liposome solution (1.0 mM POPC, 300 mM internal KCl, 300 mM external KGlu) at t = 15 s, followed by monensin (0.1 mol%) from DMSO at t = 30 s, and an aqueous Triton-X solution at t = 360 s. Blank experiments were also performed in which MeOH (without transporter) was added. (left) performed at pH = 7.2 and (right) performed at pH = 5.5.

In-Situ photodeactivation of (*Z*)-1

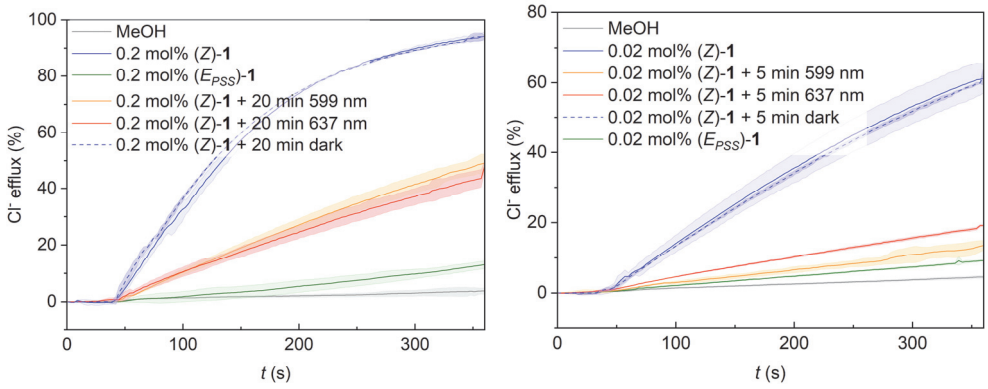

Figure E17. (left) Chloride efflux plotted versus time as measured by a chloride selective electrode in the monensin-coupled assay at pH 7.2. For the *in situ* irradiated samples the transporter was added to the liposome prior to assay, and irradiated for 20 minutes. An identical sample was prepared and kept in the dark for the same amount of time. Blank experiments were also performed in which MeOH (without transporter) was added. (right) Chloride efflux plotted versus time as measured by a chloride-selective electrode in the monensin-coupled assay at pH 5.5. For the *in situ* irradiated samples, the transporter was added to the liposome prior to assay, and irradiated for 5 minutes. An identical sample was prepared and kept in the dark for the same amount of time. Blank experiments were also performed in which MeOH (without transporter) was added.

UV-Vis studies in POPC liposomes

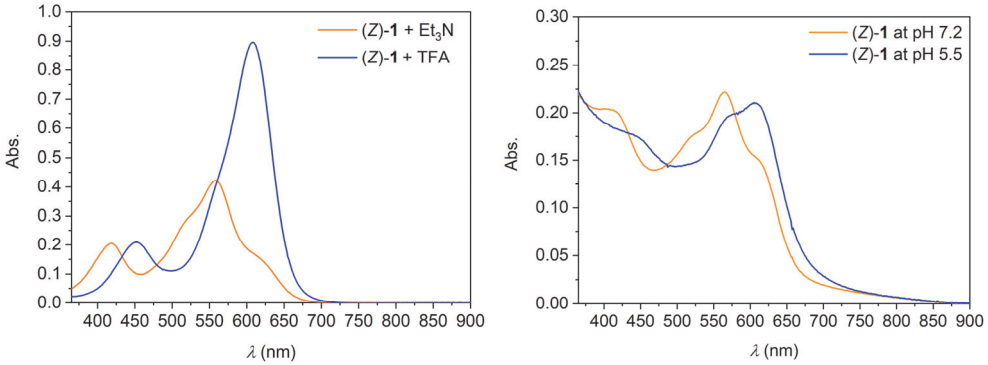

Figure E18. (left) UV-Vis spectra of (*Z*)-**1** in MeOH (15 μM, 273 K) in presence of either 3 equiv. Et_3N or 3 equiv. TFA. (right) UV-Vis spectra of 1 mol% (*Z*)-**1** in POPC liposomes (1 mM POPC, 300 mM KGlu external solution and 300 mM KCl internal solution) prepared using either 5 mM MES buffer at pH 5.5 or 5 mM HEPES buffer at pH 7.2.

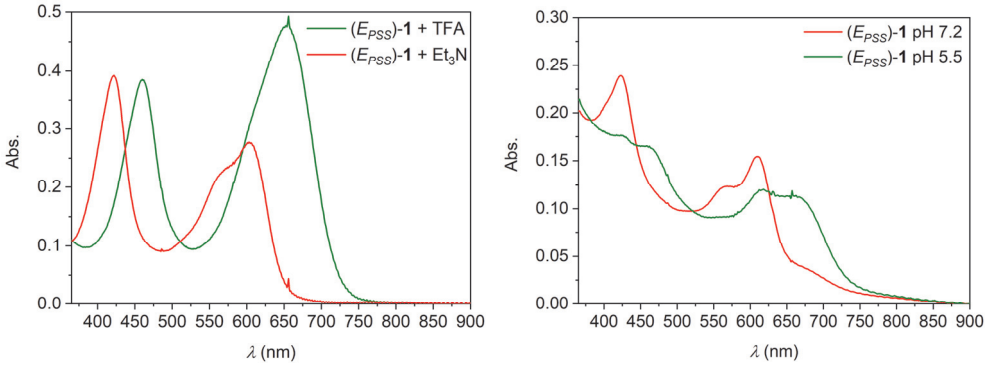

Figure E19. (left) Photogenerated (E_{PSS})-**1**·H^+ (PSS 599 nm) in MeOH (15 μM, 3 equiv. TFA, 273 K) neutralized with Et_3N (10 equiv.).(right) UV-Vis spectra of 1 mol% (E_{PSS})-**1** (pre-generated photochemically from a 1 mM solution in MeOH by irradiation with 599 nm light) in POPC liposomes (1 mM POPC, 300 mM KGlu external solution and 300 mM KCl internal solution) prepared using either 5 mM MES buffer at pH = 5.5 or 5 mM HEPES buffer at pH = 7.2.

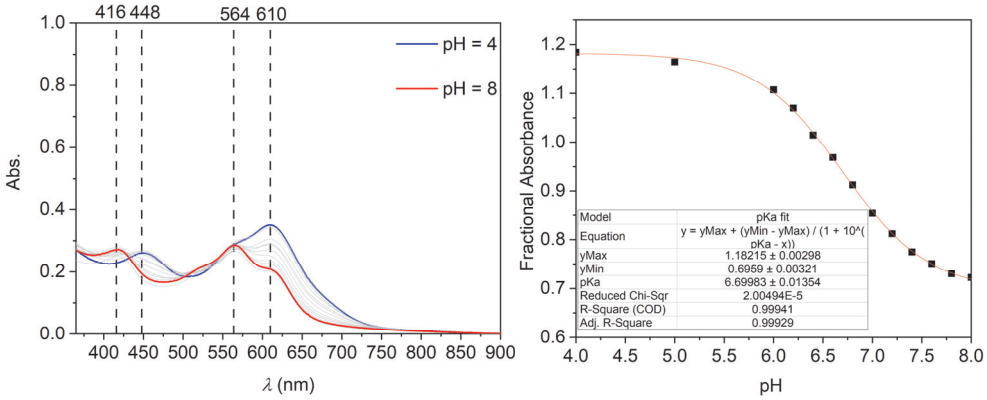

Figure E20. (left) UV-Vis spectra of POPC liposomes (1 mM, 300 mM KCl, 5 mM MES buffer pH 5.5) dissolved in an external solution with varying pH (10 mM citrate buffer from pH 4 to pH 5, 10 mM phosphate buffer for pH 6 to pH 8, with 300 mM KCl), after which 1 mol % (*Z*)-**1** was added from a MeOH solution (1 mM). Each spectrum is an individually prepared sample. (Right) Fractional absorbance [(610+448)/(416+564)] is followed over the pH range, and fitted to a sigmoidal function which affords an apparent pK_a of 6.7.

Photoisomerization in POPC liposomes

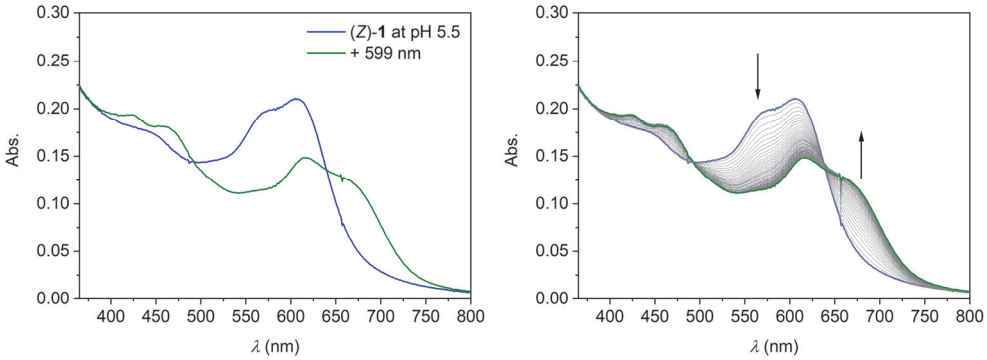

Figure E21. (Left) UV-Vis spectra of 1 mol% (*Z*)- **1** in POPC liposomes (1 mM POPC, 10 μM (*Z*)-**1** in 5 mM MES buffer pH = 5.5, 300 mM KGlu external solution and 300 mM KCl internal solution) before and after irradiation with 599 nm light. (Right) Spectral changes followed over time (5 s interval) upon irradiation with 599 nm light.

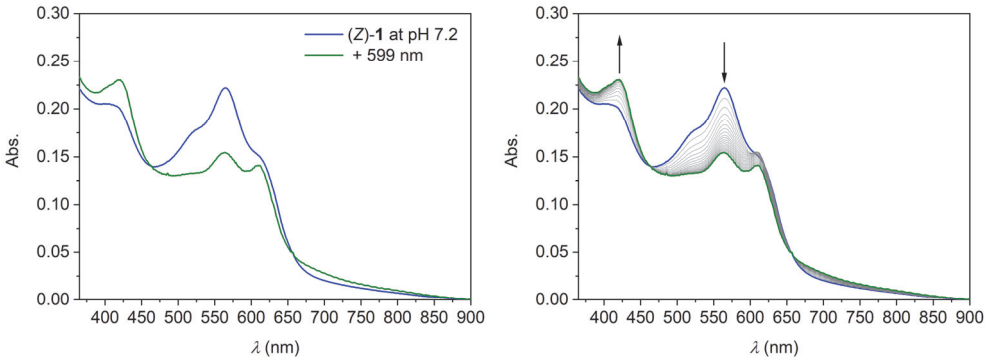

Figure E22.(Left) UV-Vis spectra of 1 mol% (*Z*)- **1** in POPC liposomes (1 mM POPC, 10 μM (*Z*)-**1** in 5 mM HEPES buffer pH = 7.2, 300 mM KGlu external solution and 300 mM KCl internal solution) before and after irradiation with 599 nm light. (Right) Spectral changes followed over time (60 s interval) upon irradiation with 599 nm light.

DFT Calculations

All calculations were performed using Gaussian 16[55], and data was visualized using Avogadro 1.2.0[56] and Gaussview 6[57]. Initial conformational searches were performed using CREST[58]. The lowest energy conformers were subsequently optimized at the B3LYP-D3/cc-pVDZ level of theory (IEFPCM MeOH), followed by the B3LYP-D3/aug-cc-pVTZ level of theory (IEFPCM MeOH). All computed stationary points were subjected to frequency analysis and confirmed as local minima (no imaginary frequencies found for all minima).

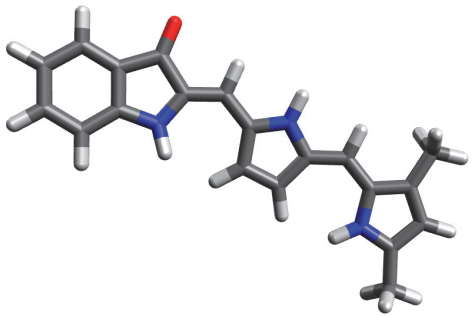

Figure E23. The optimized geometry of (Z)-**1**·H^+ calculated at B3LYP GD3 aug-cc-pVTZ level of theory with an IEFPCM MeOH solvent model. Color codes: O = red; N = blue.

Calculated coordinates can be downloaded from:
https://onlinelibrary.wiley.com/doi/10.1002/anie.202515930

5.9 References

[1] J. T. Davis, P. A. Gale, R. Quesada, *Chem. Soc. Rev.* **2020**, *49*, 6056–6086.

[2] A. Mondal, M. Ahmad, D. Mondal, P. Talukdar, *Chem. Commun.* **2023**, *59*, 1917–1938.

[3] E. Feo, P. A. Gale, *Curr. Opin. Chem. Biol.* **2024**, *83*, 102535.

[4] H. Li, J. J. Salomon, D. N. Sheppard, M. A. Mall, L. J. V. Galietta, *Curr. Opin. Pharmacol.* **2017**, *34*, 91–97.

[5] H. Li, H. Valkenier, A. G. Thorne, C. M. Dias, J. A. Cooper, M. Kieffer, N. Busschaert, P. A. Gale, D. N. Sheppard, A. P. Davis, *Chem. Sci.* **2019**, *10*, 9663–9672.

[6] R. Quesada, R. Dutzler, *J. Cystic Fibrosis* **2020**, *19*, S37–S41.

[7] S.-K. Ko, S. K. Kim, S. Share, V. M. Lynch, J. Park, W. Namkung, W. Van Rossom, N. Busschaert, P. A. Gale, J. L. Sessler, I. Shin, *Nat. Chem.* **2014**, *6*, 885–892.

[8] E. Hernando, V. Soto-Cerrato, S. Cortés-Arroyo, R. Pérez-Tomás, R. Quesada, *Org. Biomol. Chem.* **2014**, *12*, 1771–1778.

[9] S.-H. Park, S.-H. Park, E. N. W. Howe, J. Y. Hyun, L.-J. Chen, I. Hwang, G. Vargas-Zuñiga, N. Busschaert, P. A. Gale, J. L. Sessler, I. Shin, *Chem* **2019**, *5*, 2079–2098.

[10] L. E. Brennan, L. K. Kumawat, M. E. Piatek, A. J. Kinross, D. A. McNaughton, L. Marchetti, C. Geraghty, C. Wynne, H. Tong, O. N. Kavanagh, F. O'Sullivan, C. S. Hawes, P. A. Gale, K. Kavanagh, R. B. P. Elmes, *Chem* **2023**, *9*, 3138–3158.

[11] T. Sato, H. Konno, Y. Tanaka, T. Kataoka, K. Nagai, H. H. Wasserman, S. Ohkuma, *J. Biol. Chem.* **1998**, *273*, 21455–21462.

[12] J. L. Sessler, L. R. Eller, W.-S. Cho, S. Nicolaou, A. Aguilar, J. T. Lee, V. M. Lynch, D. J. Magda, *Angew. Chem. Int. Ed.* **2005**, *44*, 5989–5992.

[13] J. L. Seganish, J. T. Davis, *Chem. Commun.* **2005**, 5781–5783.

[14] B. Díaz de Greñu, P. I. Hernández, M. Espona, D. Quiñonero, M. E. Light, T. Torroba, R. Pérez-Tomás, R. Quesada, *Chem. Eur. J.* **2011**, *17*, 14074–14083.

[15] W. Rossom, D. J. Asby, A. Tavassoli, P. A. Gale, *Org. Biomol. Chem.* **2016**, *14*, 2645–2650.

[16] L. A. Jowett, E. N. W. Howe, V. Soto-Cerrato, W. Van Rossom, R. Pérez-Tomás, P. A. Gale, *Sci. Rep.* **2017**, *7*, 9397.

[17] N. Busschaert, R. B. P. Elmes, D. D. Czech, X. Wu, I. L. Kirby, E. M. Peck, K. D. Hendzel, S. K. Shaw, B. Chan, B. D. Smith, K. A. Jolliffe, P. A. Gale, *Chem. Sci.* **2014**, *5*, 3617–3626.

[18] R. B. P. Elmes, N. Busschaert, D. D. Czech, P. A. Gale, K. A. Jolliffe, *Chem. Commun.* **2015**, *51*, 10107–10110.

[19] S. V. Shinde, P. Talukdar, *Angew. Chem. Int. Ed.* **2017**, *56*, 4238–4242.

[20] A. Saha, N. Akhtar, V. Kumar, S. Kumar, H. K. Srivastava, S. Kumar, D. Manna, *Org. Biomol. Chem.* **2019**, *17*, 5779–5788.

[21] L. Tapia, Y. Pérez, M. Bolte, J. Casas, J. Solá, R. Quesada, I. Alfonso, *Angew. Chem. Int. Ed.* **2019**, *58*, 12465–12468.

[22] S. V. Shinde, P. Talukdar, *Org. Biomol. Chem.* **2019**, *17*, 4483–4490.

[23] P. V. Santacroce, J. T. Davis, M. E. Light, P. A. Gale, J. C. Iglesias-Sánchez, P. Prados, R. Quesada, *J. Am. Chem. Soc.* **2007**, *129*, 1886–1887.
[24] E. N. W. Howe, N. Busschaert, X. Wu, S. N. Berry, J. Ho, M. E. Light, D. D. Czech, H. A. Klein, J. A. Kitchen, P. A. Gale, *J. Am. Chem. Soc.* **2016**, *138*, 8301–8308.
[25] A. Castellano-Hinojosa, M. J. Gallardo-Altamirano, J. González-López, A. González-Martínez, *J. Hazard. Mater.* **2023**, *447*, 130818.
[26] W. A. Velema, W. Szymanski, B. L. Feringa, *J. Am. Chem. Soc.* **2014**, *136*, 2178–2191.
[27] K. Hüll, J. Morstein, D. Trauner, *Chem. Rev.* **2018**, *118*, 10710–10747.
[28] W. Lee, Z.-H. Li, S. Vakulenko, S. Mobashery, *J. Med. Chem.* **2000**, *43*, 128–132.
[29] W. A. Velema, J. P. van der Berg, M. J. Hansen, W. Szymanski, A. J. M. Driessen, B. L. Feringa, *Nat. Chem.* **2013**, *5*, 924–928.
[30] M. Borowiak, W. Nahaboo, M. Reynders, K. Nekolla, P. Jalinot, J. Hasserodt, M. Rehberg, M. Delattre, S. Zahler, A. Vollmar, D. Trauner, O. Thorn-Seshold, *Cell* **2015**, *162*, 403–411.
[31] J. de Jong, J. E. Bos, S. J. Wezenberg, *Chem. Rev.* **2023**, *123*, 8530–8574.
[32] M. Ahmad, S. A. Gartland, M. J. Langton, *Angew. Chem. Int. Ed.* **2023**, *62*, e202308842.
[33] Y. R. Choi, G. C. Kim, H.-G. Jeon, J. Park, W. Namkung, K.-S. Jeong, *Chem. Commun.* **2014**, *50*, 15305–15308.
[34] A. Kerckhoffs, M. J. Langton, *Chem. Sci.* **2020**, *11*, 6325–6331.
[35] M. Ahmad, S. Chattopadhayay, D. Mondal, T. Vijayakanth, P. Talukdar, *Org. Lett.* **2021**, *23*, 7319–7324.
[36] S. J. Wezenberg, L. J. Chen, J. E. Bos, B. L. Feringa, E. N. W. Howe, X. Wu, M. A. Siegler, P. A. Gale, *J. Am. Chem. Soc.* **2022**, *144*, 331–338.
[37] J. E. Bos, M. A. Siegler, S. J. Wezenberg, *J. Am. Chem. Soc.* **2024**, *146*, 31085–31093.
[38] P. Ferreira, G. Aragay, P. Ballester, *Org. Chem. Front.* **2024**, *11*, 2468–2476.
[39] Z. Kokan and M. J. Chmielewski, *J. Am. Chem. Soc.* **2018**, *140*, 16010–16014.
[40] J. de Jong, B. L. Feringa, S. J. Wezenberg, *ChemPhysChem* **2019**, *20*, 3306–3310.
[41] B. Shao, H. Fu, I. Aprahamian, *Science* **2024**, *385*, 544–549.
[42] M. Vega, L. Martínez-Crespo, M. Barceló-Oliver, C. Rotger, A. Costa, *Org. Lett.* **2023**, *25*, 3423–3428.
[43] M. Ikegami, T. Arai, *Bull. Chem. Soc. Jpn.* **2003**, *76*, 1783–1792.
[44] V. Josef, F. Hampel, H. Dube, *Angew. Chem. Int. Ed.* **2022**, *61*, e202210855.
[45] M. Krell-Jørgensen, H. Zulfikri, M. G. Bonnevie, F. S. Bro, A. O. Dohn, L. Laraia, *Chem. Commun.* **2023**, *59*, 563–566.
[46] N. Duindam, M. van Dongen, M. A. Siegler, S. J. Wezenberg, *J. Am. Chem. Soc.* **2023**, *145*, 21020–21026.
[47] T. Arai, M. Ikegami, *Chem. Lett.* **1999**, *28*, 965–966.
[48] T. E. Wood, A. Thompson, *Chem. Rev.* **2007**, *107*, 1831–1861.
[49] J. A. van Koeveringe, J. Lugtenburg, *Recl. Trav. Chim. Pays-Bas* **1977**, *96*, 55–57.

[50] C. Wan, A. Burghart, J. Chen, F. Bergström, L. B. Å. Johansson, M. F. Wolford, T. G. Kim, M. R. Topp, R. M. Hochstrasser, K. Burgess, *Chem. Eur. J.* **2003**, *9*, 4430–4441.

[51] C. Uriel, D. Grenier, F. Herranz, N. Casado, J. Bañuelos, E. Rebollar, I. Garcia-Moreno, A. M. Gomez, J. C. López, *J. Org. Chem.* **2024**, *89*, 4042–4055.

[52] C. Petermayer, H. Dube, *Acc. Chem. Res.* **2018**, *51*, 1153–1163.

[53] C. Frassineti, S. Ghelli, P. Gans, A. Sabatini, M. S. Moruzzi, A. Vacca, *Anal. Biochem.* **1995**, *231*, 374–382.

[54] X. Wu, E. N. W. Howe, P. A. Gale, *Acc. Chem. Res.* **2018**, *51*, 1870–1879.

[55] Gaussian 16, Revision C.01, M. J. Frisch, G. W. Trucks, H. B. Schlegel, G. E. Scuseria, M. A. Robb, J. R. Cheeseman, G. Scalmani, V. Barone, G. A. Petersson, H. Nakatsuji, X. Li, M. Caricato, A. V. Marenich, J. Bloino, B. G. Janesko, R. Gomperts, B. Mennucci, H. P. Hratchian, J. V. Ortiz, A. F. Izmaylov, J. L. Sonnenberg, D. Williams-Young, F. Ding, F. Lipparini, F. Egidi, J. Goings, B. Peng, A. Petrone, T. Henderson, D. Ranasinghe, V. G. Zakrzewski, J. Gao, N. Rega, G. Zheng, W. Liang, M. Hada, M. Ehara, K. Toyota, R. Fukuda, J. Hasegawa, M. Ishida, T. Nakajima, Y. Honda, O. Kitao, H. Nakai, T. Vreven, K. Throssell, J. A. Montgomery, Jr., J. E. Peralta, F. Ogliaro, M. J. Bearpark, J. J. Heyd, E. N. Brothers, K. N. Kudin, V. N. Staroverov, T. A. Keith, R. Kobayashi, J. Normand, K. Raghavachari, A. P. Rendell, J. C. Burant, S. S. Iyengar, J. Tomasi, M. Cossi, J. M. Millam, M. Klene, C. Adamo, R. Cammi, J. W. Ochterski, R. L. Martin, K. Morokuma, O. Farkas, J. B. Foresman, and D. J. Fox, Gaussian, Inc., Wallingford CT, 2016.

[56] Avogadro: an open-source molecular builder and visualization tool. Version 1.2.0 http://avogadro.cc/.

[57] GaussView, Version 6, R. Dennington, T. A. Keith, J. M. Millam, Semichem Inc., Shawnee Mission, KS, 2016.

[58] P. Pracht, F. Bohle, S. Grimme, *Phys. Chem. Chem. Phys.* **2020**, *22*, 7169–7192.